Strain-induced ferroelectricity and piezoelectricity in centrosymmetric binary oxides

Xiaoqing Yang [1,2,3,*] Chao Liu [1,2,3,*] Le Fang,[1,2,3,*] Tianhao Su [1,2,3] Minglang Hu,[1,2,3] Yangyang Chen,[1,2,3,†] Bin Zhou,[2] Haijun Su,[4] Xiangyang Kong,[5,‡] Laurent Bellaiche,[6] and Wei Ren[1,2,3,§]

[1]*Physics Department, Materials Genome Institute, State Key Laboratory of Advanced Special Steel, Shanghai Key Laboratory of High Temperature Superconductors, International Center for Quantum and Molecular Structures, Shanghai University, Shanghai 200444, China*
[2]*Hubei Key Laboratory of Ferro & Piezoelectric Materials and Devices, Hubei University, Wuhan 430062, China*
[3]*Zhejiang Laboratory, Hangzhou 311100, China*
[4]*State Key Laboratory of Solidification Processing, Northwestern Polytechnical, University, Xi'an 710072, China*
[5]*Institute of Materials for Mobile Energy, School of Materials Science and Engineering, Shanghai Jiao Tong University, Shanghai 200240, China*
[6]*Physics Department and Institute for Nanoscience and Engineering, University of Arkansas, Fayetteville, Arkansas 72701, USA*

First-principles calculations are performed to predict ferroelectricity in the binary rocksalt oxide family (AO with A = Cd, Ba, Sr, Ca, Mg, etc.) via the application of biaxial strain. The origins of such ferroelectricity are discussed from the lattice dynamics perspective and electronic structure properties. Under compressive strain, the strikingly large longitudinal piezoelectric effect is induced due to the deformation along the c direction as a response to the stress. These findings have the potential to motivate the search of new simple binary oxides possessing ferroelectricity that may lead to novel devices.

I. INTRODUCTION

To date, ferroelectricity (FE) in the class of simple binary materials has attracted a considerable interest for multifunctional applications. Specifically, FE ordering in the rocksalt oxides is predicted by using first-principles density functional calculations [1]. Reference [2] indicated that ferroelectricity could indeed be induced in ferromagnetic rocksalt EuO by using epitaxial strain—which thus makes it multiferroic [3]. Experimentally, strain can be tuned through lattice mismatch on a suitable substrate, by stretching the film, or via chemical dopants [4,5]. External strain has been exploited to induce novel metal-insulator transitions [6] and polar-nonpolar transitions in layered oxides [7]. Moreover, with positive strain along the c direction, an electric field can induce chemical expansion and high piezoelectricity in initially centrosymmetric oxygen-nonstoichiometric oxide Gd-doped CeO_{2-x} [8].

Inspired by these pioneering works, we explore the ferroelectricity in simple rocksalt AO (A = Cd, Ba, Sr, Ca, Mg, etc.) crystals, and the origin of large longitudinal piezoelectric effect as well. Simple binary oxides adopting a rocksalt structure have a center inversion symmetry that prevents the existence of a spontaneous polarization. Herein, we present the possible occurrence of ferroelectricity and piezoelectricity in simple strained-binary oxides AO. The lattice strain is expressed as $\eta = (a - a_0)/a_0$ and varies from 0% to −9%. First, we focus on the biaxial strain engineering with the

nonpolar to polar phase transition of AO from cubic (space group $Fm\bar{3}m$, no. 225) to a noncentrosymmetric structure ($I4mm$, no. 107). Furthermore, we reveal the consequence of this transition by calculating properties under epitaxial strain using first principles. These AOs exhibit longitudinal piezoelectricity in the emerging FE phase, and the piezoelectricity is strongly sensitive to applied strain. This work predicts the ferroelectricity and piezoelectricity of rocksalt CdO (note that other strained BaO, SrO, CaO, MgO oxides were previously reported to possess ferroelectricity [1,9]).

II. COMPUTATIONAL METHOD

We perform density function theory (DFT) [10] computations implemented within Vienna Ab initio Simulation Package (VASP) [11], by using the projector augmented-wave (PAW) [12,13] pseudopotentials with the Perdew-Burke-Ernzerhof (PBE) [14] functional method for the exchange-correlation potential. For all calculations, the valence state configurations are taken as $5s^2 4d^{10}$ for Cd, $5s^2 5p^6 6s^2$ for Ba, $4s^2 4p^6 5s^2$ for Sr, $3s^2 3p^6 4s^2$ for Ca, $3s^2$ for Mg and $2s^2 2p^4$ for O. To better describe the electronic correlations in the Cd $4d$ shell, the GGA (generalized gradient approximation) + U method [15] with $U_{\text{eff}} = 2.34$ eV is used [16,17] (for the other AO systems, namely BaO, CaO, SrO, and MgO, no U_{eff} is used). A high convergence is obtained with a plane wave energy cutoff of 600 eV, a convergence criterion for energy of 10^{-9} eV, and a grid of $10 \times 10 \times 10$ Gamma-centered k points to sample the Brillouin zone. The structures are fully optimized until the residual Hellman-Feynman forces are less than 10^{-4} eV Å^{-1}. Band structures and density of states are calculated using a screened hybrid functional described by Heyd, Scuseria, and Ernzerhof (HSE06) [18,19]. Furthermore, the

---
*These authors contributed equally to this work.
†phycyy@shu.edu.cn
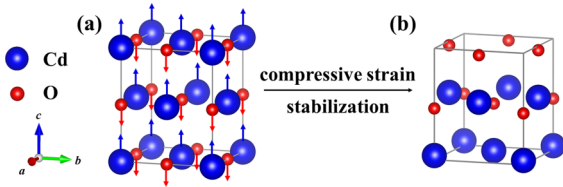‡xykong@sjtu.edu.cn
§renwei@shu.edu.cn

FIG. 1. Schematic diagrams of the rocksalt structure CdO of (a) paraelectric (PE) and (b) ferroelectric (FE) phases. The blue and red arrows represent the moving directions of the Cd and O atoms.

Born effective charges, dielectric tensors, and piezoelectric constants are calculated using density functional perturbation theory (DFPT) [20]. We apply the Berry-phase formalism of the modern polarization theory to calculate the spontaneous polarization [21]. The phonon spectra are computed based on the $2 \times 2 \times 2$ supercell using the PHONOPY [22] module and DFPT method.

III. RESULTS AND DISCUSSION

We first show the detailed structure of CdO as an example, since all cubic AO oxides are similar. By applying biaxial strain on the cubic CdO structure, an unusual FE phase is in fact induced. The initial structure of cubic CdO ($Fm\bar{3}m$) is shown in Fig. 1(a), where the blue and red spheres represent Cd and O atoms, respectively. The calculated lattice constant ($a = b = c$) for the rocksalt CdO is 4.76 Å, and is therefore in excellent agreement with the experimental value of 4.77 Å [23,24]. Under a moderate external biaxial strain, the cubic phase transforms into a tetragonal one ($I4/mmm$, no. 139) which still maintains centrosymmetry. At a critical epitaxial strain of -4.7%, a ferroelectric phase transition (from $I4/mmm$ to $I4mm$) is predicted with the Cd and O atoms that are initially in the same ab plane breaking the inversion symmetry along the c direction as shown in Fig. 1(b). Other simple AOs are in a similar situation: critical compressive strains that induce novel and mechanical stable FE phase are -4.7% (CdO), -3% (BaO), -6.3% (SrO), -7% (CaO), and -7.2% (MgO) respectively. The results of these latter four cases are similar to previously published calculations [1]. Note that the elastic modulus is one of the key parameters in materials engineering and mechanics. The elastic tensors that satisfy the Born stability criteria (in Table S1 of the Supplemental Material [25]) confirm that strained-AOs are mechanically stable [26]. Additionally, the AO systems have also a good thermal stability with the geometries still maintained without broken bonds or phase transition at 300 K; the corresponding fluctuations of total energies for 10 000 fs are plotted in Fig. S1 of the Supplemental Material [25].

The origin of the existence of the FE phase can be explained from the lattice dynamics perspective, which is described in terms of a displacive FE transition. A softened optical phonon is a typical signature for a displacive FE phase transition. The transverse optical (TO) mode frequency depends on two contributions: short-range and long-range Coulomb interactions. When the long-range Coulomb interactions favoring the FE phase is large enough to compensate the short-range resilience favoring the undistorted PE structure, the atoms move towards new stable positions (FE phase) with
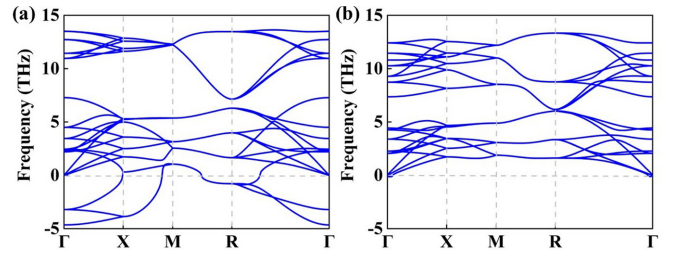

FIG. 2. Phonon spectra for CdO of (a) PE $I4/mmm$ phase and (b) FE $I4mm$ phase. The PE imaginary frequencies located at the Γ point corresponding to the unstable phonon modes are eliminated by a phase transition to FE state with a polarization along the c direction.

the positive and negative ions moving in opposite directions, making the uniform spontaneous polarization appearing in the entire crystal. As shown in Fig. 2(a), the eigenvector of the unstable phonon mode at the Γ center of the Brillouin zone (see Fig. S2 in the Supplemental Material [25]) represents an identical atomic displacement pattern in each unit cell, and is associated with an FE polarization. Note that the imaginary frequencies located at the Γ point in Fig. 2(a) correspond to displacements all occurring along the c direction. Additionally, the phonon spectrum of the strained FE state, shown in Fig. 2(b) without any imaginary modes, proves that the FE CdO state is dynamically stable.

It is well known that the PBE functional underestimates the band gap severely and cannot describe the electronic properties accurately, while the hybrid functional is more accurate in predicting band structures [27,28]. Consequently, in order to get insight of the FE and PE structures, we perform hybrid functional computations to investigate the partial density of states (PDOS) of CdO. Figure 3 displays the PDOS for Cd p, d, and O p orbitals which contribute quite differently in the PE and FE tetragonal states. Comparing the PDOS near the Fermi energy between these PE and FE states, we find that the overlapping densities of the occupied p_z and d_{z^2} orbitals of the Cd atom both increase and the p_z orbital of O atom remains the most occupied state in the FE phase. The above orbitals contribute mainly along the c direction. The bonding mechanism of CdO is that Cd p_z and d_{z^2} orbitals self-mix and then hybridize with the O p_z orbital, resulting in atomic off-center displacement along the c direction and the emergence of the FE phase. Such a microscopic mechanism was also proposed in the studies of FE ZnMgO$_2$ and β-CuGaO$_2$, with full d orbitals [29,30].

Electronic properties, such as the difference in energy or orbital contribution between the conduction band minimum (CBM) and valence band maximum (VBM) are also strain dependent. Here we present band structures when employing HSE06 to obtain the electronic structure of CdO with a band gap close to that of the experiment. The result indicates that the electronic band gap (indirect) of rocksalt CdO is 0.8 eV and the direct band gap at the Γ point is 2.0 eV [Fig. 4(b)], both in excellent agreement with values determined previously [17,31–33]. With such indirect forbidden bandwidth corresponding to the wavelength of the visible light, CdO is suitable for optical devices like infrared detectors, photodiodes, and sensors [34–36]. Figure 4(a) further reveals the
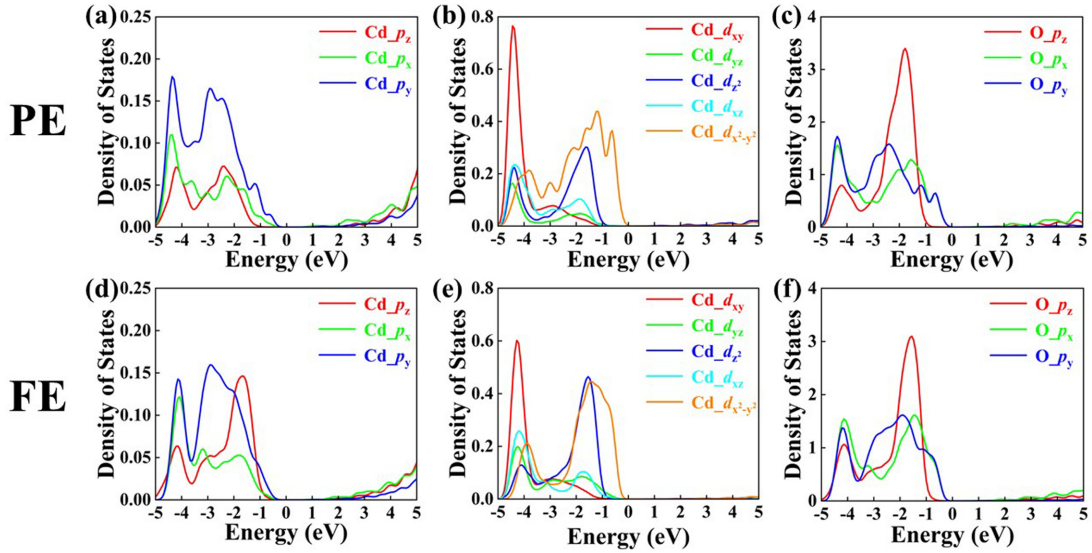
FIG. 3. Partial density of states (PDOS) for Cd p, d, and O p orbitals by using the hybrid functional (HSE06) method. Panels (a)–(c) are for the PE $I4/mmm$ phase and (d)–(f) are for the FE $I4mm$ phase.

effect of strain on the indirect band gap: the gap decreases linearly before the phase transition boundary and shows a minimum value when approaching the FE state, before enhancing monotonically with increasing strain. This change can be attributed to the shifts in bond lengths between Cd and O (shown in Fig. S3 of the Supplemental Material [25]), which directly affect the electronic property of CdO. Figure 4 also reveals the orbitals that mainly contribute to the CBM and VBM under different strains. We find that in the cubic structure without any strain [Fig. 4(b)], the VBM is mainly contributed by all the p orbitals of the O atoms. When the strain is applied, the VBM becomes only constituted by p_x and p_y orbitals. As for the CBM, it always keeps contributions from the s orbitals of both Cd and O.
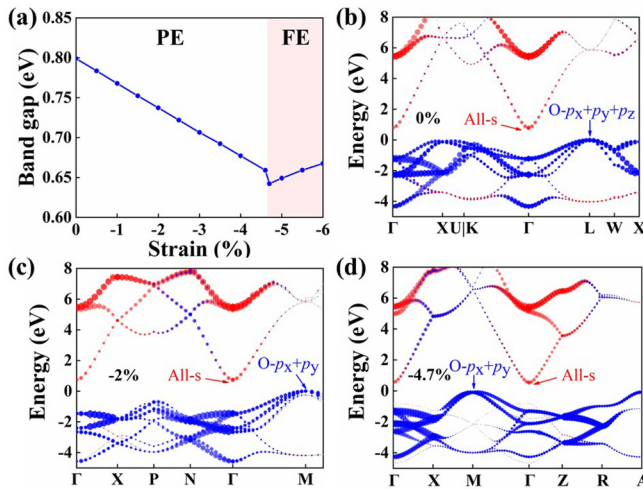

FIG. 4. (a) HSE electronic band gap of CdO as a function of the compressive strain ranged between 0 and −6%. The projected energy band structures with the compressive strain values of (b) 0%, (c) −2%, and (d) −4.7%.

Spontaneous polarization and polarization switching barrier values are among the most significant properties of ferroelectricity. Let us thus now present FE characteristics of BaO, CdO, and SrO, as they require smaller magnitude of strains to induce ferroelectricity. Figure 5 displays the evolution of the energy versus polarization in these three systems. The two points with the lowest energy are the equilibrium ferroelectric states with opposite polarization directions. When these two equivalent polar states switch under an external electric field, ferroelectrics have to cross an energy barrier through the PE point. We find that the potential barriers are 40, 76, and 119 meV/formula unit (f.u.), and the equilibrium polarizations are 29, 54, and 48 μC/cm^2, respectively, for BaO, CdO, and SrO. The spontaneous polarizations and depths of the double well of CdO and SrO are quite comparable to those of typical perovskite ferroelectrics such as BaTiO$_3$ [37,38]. Interestingly, the barrier we get for strained-rocksalt CdO is about 1/3 of wurtzite CdO (210 meV/f.u.) [39], which implies that such practical FE material with low coercive voltage can be useful in ferroelectric memory devices.

We now evaluate the effect of epitaxial strain on the dielectric response and Born effective charge, in addition to spontaneous FE polarization and barriers of polarization switching. Figure 6(a) shows the effect of strain on the static dielectric tensor ε^{zz}. In the strain-free case, the dielectric tensor is isotropic because of the cubic structure. The dielectric permittivity ε^{zz} changes slowly under the strain away from the phase transition boundary, while increasing dramatically at this boundary up to over 500 [shown in Fig. 6(a)]. This behavior is attributed to the PE to FE phase transition. More precisely, the compressive strain causes softening of TO modes, resulting in a sharp increase of dielectric permittivity along the c direction [40]. Figure 6(b) displays the strain-dependent evolution of the Born effective charge of Cd (which is equal in magnitude and opposite in sign to that of the O atom). The Born effective charge is isotropic in a cubic lattice, and becomes a tensor in a noncubic lattice under strain [41]. Since the FE spontaneous polarization of CdO is along the z
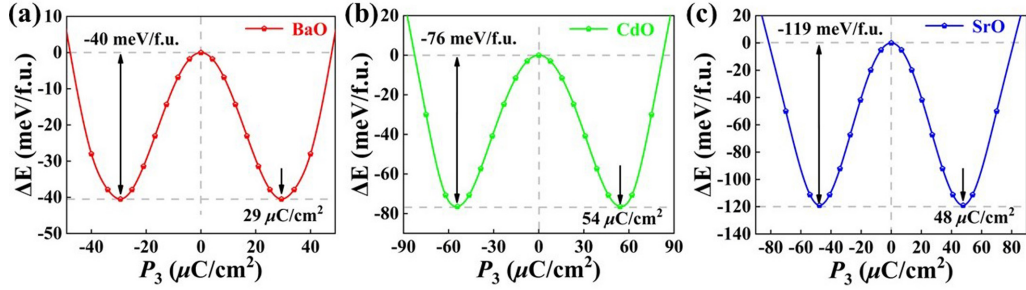
FIG. 5. Energy versus polarization for (a) BaO at -3% strain, (b) CdO at -4.7% strain, and (c) SrO at -6.3% strain (all these compressive strains are the critical ones associated with the phase transition).

axis, we consider the Born effective charge Z_{33} in Fig. 6(b). One can see that Z_{33} first decreases with strain in the $I4/mmm$ phase as the ions shift from the high symmetry cubic sites, and exhibits a drop at the phase transition within the FE state, and then increases with the strain strength.

Varying the lattice strain allows the creation of an electrical polarization from a cubic crystal material. Figure 6(c) presents the value of polarization (P_3) as a function of compressive strain by using the Berry-phase theory. Above the critical point, P_3 displays an abrupt change and increases upon increasing compressive strain, whereas P_3 is null for all strains within the $I4/mmm$ PE phase. The dramatic jump change of P_3 near the critical point indicates that the PE to FE transition is of the first order. The spontaneous polarization for CdO from the Berry phase method reaches 54 μC/cm^2 at -4.7% strain, comparable to the classical FE oxide BaTiO$_3$ ($\sim 50\,\mu$C/cm^2) [42]. We also compute the strain dependence of the energy barriers for polarization switching. As shown in Fig. 6(d), the compressive strain tunes the barrier and makes the energy difference between the FE and PE states increasingly larger. The corresponding barrier for CdO at -4.7% strain is

76 meV/f.u., even lower than those of traditional perovskite ferroelectrics [37,43], suggesting a promising FE device candidate with high endurance and reasonably low barrier.

Furthermore, piezoelectrics form a class of dielectric materials which can be polarized by not only electric field, but also the application of mechanical stress. Piezoelectric devices are able to convert electrical energy to mechanical energy and vice versa, and are thus an important player for energy conversion and signal transmission. Another appealing property of FE AO compounds is that they possess a rather large piezoelectric response. The piezoelectric modulus d_{33} is found here to be 304 pC/N for BaO, 188 pC/N for CdO, 149 pC/N for SrO, 261 pC/N for CaO, and 107 pC/N for MgO, showing superior piezoelectric response than other known piezoelectric materials including hexagonal zinc oxide ZnO (12.4 pC/N) [44], LiMgP (25 pC/N) [45], and ScAlN (24.6 pC/N) [46,47].

To better understand the underlying mechanism of the anomalous piezoelectric response, we focus on the d_{ij} piezoelectric modulus. Reflecting the ability to mutually transform mechanical energy and electrical energy, it is obtained through the thermodynamic relationship between e_{ik} and S_{kj} matrices [48]:

$$d_{ij} = e_{ik}S_{kj},$$

where e_{ik} is the piezoelectric constant that links the induced polarization in direction i with an applied strain with component k. S_{kj} is the elastic compliance tensor [49], which relates the deformation produced by the application of a stress. That is to say, the piezoelectric modulus d_{ij} involves an intercoupling of electric and elastic phenomena. The crystallographic symmetry is important for piezoelectricity, with the e_{ik} and S_{kj} matrices for the $I4mm$ space group being

$$e_{ik} = \begin{bmatrix} 0 & 0 & 0 & 0 & e_{15} & 0 \\ 0 & 0 & 0 & e_{15} & 0 & 0 \\ e_{31} & e_{31} & e_{33} & 0 & 0 & 0 \end{bmatrix},$$

$$S_{kj} = \begin{bmatrix} S_{11} & S_{12} & S_{13} & 0 & 0 & 0 \\ S_{12} & S_{11} & S_{13} & 0 & 0 & 0 \\ S_{13} & S_{13} & S_{33} & 0 & 0 & 0 \\ 0 & 0 & 0 & S_{44} & 0 & 0 \\ 0 & 0 & 0 & 0 & S_{44} & 0 \\ 0 & 0 & 0 & 0 & 0 & S_{66} \end{bmatrix}.$$
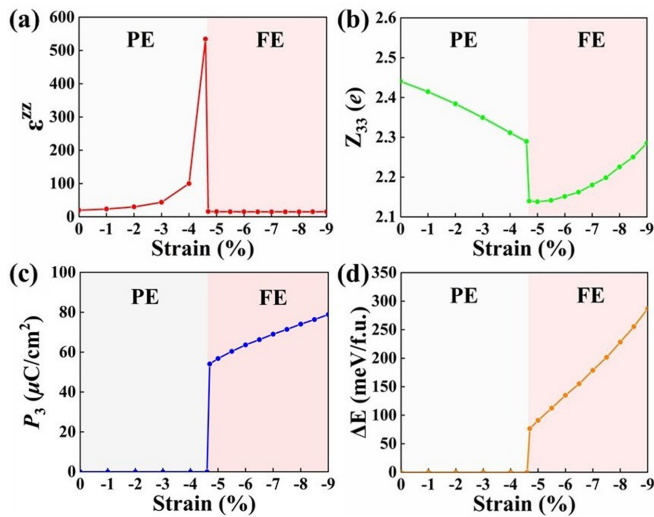

FIG. 6. Physical properties of CdO as function of compressive strain: (a) dielectric permittivity along the c direction; (b) Born effective charge Z_{33}; (c) spontaneous polarization in the c direction; (d) energy barrier for polarization switching.
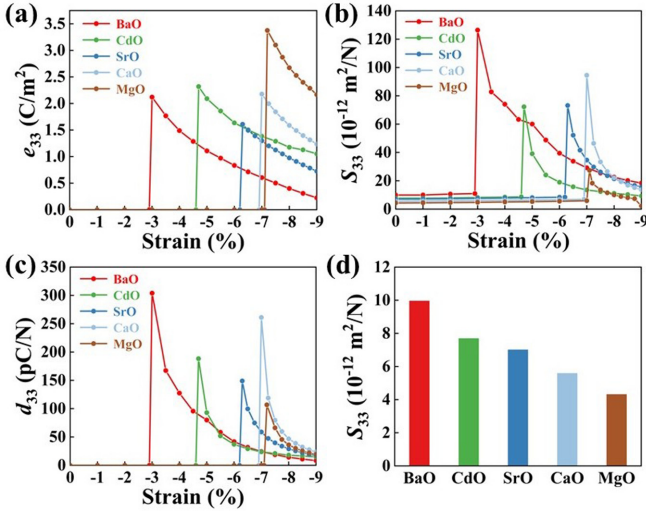
FIG. 7. The calculated (a) piezoelectric constant, (b) elastic compliance tensor, (c) piezoelectric modulus of AO as function of the epitaxial compressive strain (from 0 to -9%), and (d) elastic compliance tensor of AO under 0% strain.

With the above relationship and forms of e_{ik} and S_{kj}, the longitudinal piezoelectric modulus d_{33} can be expressed as

$$d_{33} = 2e_{31}S_{13} + e_{33}S_{33}.$$

To reveal the effect of epitaxial strain on piezoelectric response and the origin of large d_{33}, the piezoelectric constant and elastic compliance tensor are shown in Fig. 7. Note that in these piezoelectric AO systems, the second term $e_{33}S_{33}$ dominates the total piezoelectric response d_{33}, since e_{33} is several times larger than e_{31}, and S_{33} is also the largest component of the elastic compliance tensor. In Fig. 7(a), the predicted PE to FE critical strains increase in the order of BaO, CdO, SrO, CaO, and MgO, while e_{33} peaked values have a tendency to decrease under an epitaxial strain. For comparison, MgO has a more positive e_{33} than the rest of AOs. Figure 7(b) shows that S_{33} of BaO is substantially larger than others near the critical strain, and an analogous d_{33} plot is shown in Fig. 7(c). Overall, BaO has the largest d_{33} and MgO has the minimal d_{33}, and the behaviors of d_{33} are similar to S_{33}, indicating that the elastic compliance S_{33} plays an important influence role on d_{33}. The elastic compliance contributes most to the piezoelectric effects, meaning the large piezoelectric response is mainly originating from the high sensitivity of deformation to the application of a stress. We also investigate the magnitude of epitaxial strain that generates polarization from the viewpoint of elastic compliance. Figure 7(d) shows the S_{33} for rocksalt AO without epitaxial strain. The abscissa from left to right is in the order of increasing critical strain that can induce FE phase. We find that the strain value at which the FE state occurs has an anticorrelation with S_{33} of the unstrained case: the larger value of this S_{33} corresponds to the smaller phase transition strain.

Furthermore, it is known that superlattices can produce striking property enhancements as well as new combinations of desired properties by varying their layer thicknesses. We

therefore constructed superlattices to investigate if ferroelectricity can be strain engineered in different metal oxides. The proposed superlattice consists of rocksalt A_1O and A_2O buckled monolayers alternately arranged along the crystallographic c direction [shown in Fig. S4(a) of the Supplemental Material [25]]. In the following, all the epitaxial strains reported are calculated with respect to the relaxed superlattice in its PE phase. Here we consider six superlattices as a prototypical example [shown in Fig. S4(b) of the Supplemental Material [25]]. The volume ratio of MgO/SrO is 0.54, and such a large volume difference drives the phase transition to FE without any external strain. In contrast, the critical strain that can induce the FE state is relatively large (-5.6%) when their parent oxide volume ratio approaches 1. It can be verified that the minimum strain to induce ferroelectricity increases when the volumes of the two parent components become close to each other. Moreover, the critical strain of the superlattice is much less than that of their parent components. This feature makes the superlattice even more interesting and promising to be explored in other ferroelectric oxides.

It is worth mentioning that the nonpolar to polar phase transition occurs at a moderate strain, implying that these strained systems might be experimentally synthesized. As a matter of fact, strains of about $\pm3\%$ are common for epitaxial oxides in experiments nowadays, whereas a 6% biaxial strain has been achieved in EuO grown on $(LaAlO_3)_{0.29}$-$(SrAl_{1/2}Ta_{1/2}O_3)_{0.71}$ substrate and a -6.6% compressive strain has been experimentally realized in $BiFeO_3$ grown on $YAlO_3$ substrate [2,50].

IV. CONCLUSIONS

In summary, we demonstrate that tuning strain can induce giant ferroelectricity in binary oxide AO (A = Cd, Mg, Ca, Sr, Ba) and A_1O/A_2O superlattices. They possess unexpectedly low polarization barrier and ideal large polarization that are comparable to the classical ferroelectric $BaTiO_3$ perovskite. Their large longitudinal piezoelectric effect is mainly caused by the huge deformation along the c direction due to a stress, accompanied by a softened elastic compliance S_{33}. These unique properties make binary oxides AO excellent candidates for multifunctional ferroelectric devices. As increasing ferroelectric evidence has been reported in the strained-rocksalt BaO or EuO, our present work will stimulate more experimental efforts on ferroelectricity and piezoelectricity from centrosymmetric binary oxides.

[1] E. Bousquet, N. A. Spaldin, and P. Ghosez, Phys. Rev. Lett. **104**, 037601 (2010).

[2] V. Goian, R. Held, E. Bousquet, Y. Yuan, A. Melville, H. Zhou, V. Gopalan, P. Ghosez, N. A. Spaldin, D. G. Schlom *et al.*, Commun. Mater. **1**, 74 (2020).

[3] Y. Yang, W. Ren, D. Wang, and L. Bellaiche, Phys. Rev. Lett. **109**, 267602 (2012).

[4] A. Chen, Q. Su, H. Han, E. Enriquez, and Q. Jia, Adv. Mater. **31**, 1803241 (2019).

[5] J. Kim, H. Takenaka, Y. Qi, A. R. Damodaran, A. Fernandez, R. Gao, M. R. McCarter, S. Saremi, L. Chung, A. M. Rappe *et al.*, Adv. Mater. **31**, 1901060 (2019).

[6] B. Chen, N. Gauquelin, D. Jannis, D. M. Cunha, U. Halisdemir, C. Piamonteze, J. H. Lee, J. Belhadi, and F. Eltes, S. Abel *et al.*, Adv. Mater. **32**, 2004995 (2020).

[7] X. Z. Lu and J. M. Rondinelli, Nat. Mater. **15**, 951 (2016).

[8] D.-S. Park, M. Hadad, L. M. Riemer, R. Ignatans, D. Spirito, V. Esposito, V. Tileli, N. Gauquelin, and D. Chezganov, D. Jannis *et al.*, Science **375**, 653 (2022).

[9] V. B. Nascimento, B. V. da Costa, and J. P. Rino, Appl. Phys. A **126**, 744 (2020).

[10] B. Y. Tong and L. J. Sham, Phys. Rev. **144**, 1 (1966).

[11] Kresse and Hafner, Phys. Rev. B **47**, 558 (1993).

[12] P. E. Blöchl, Phys. Rev. B **50**, 17953 (1994).

[13] G. Kresse and D. Joubert, Phys. Rev. B **59**, 1758 (1999).

[14] B. Hammer, L. B. Hansen, and J. K. Nørskov, Phys. Rev. B **59**, 7413 (1999).

[15] L. Wang, T. Maxisch, and G. Ceder, Phys. Rev. B **73**, 195107 (2006).

[16] A. Janotti, D. Segev, and C. G. Van de Walle, Phys. Rev. B **74**, 045202 (2006).

[17] J. J. Mudd, T.-L. Lee, V. Muñoz-Sanjosé, J. Zúñiga-Pérez, D. J. Payne, R. G. Egdell, and C. F. McConville, Phys. Rev. B **89**, 165305 (2014).

[18] A. V. Krukau, O. A. Vydrov, A. F. Izmaylov, and G. E. Scuseria, J. Chem. Phys. **125**, 224106 (2006).

[19] J. Heyd and G. E. Scuseria, J. Chem. Phys. **120**, 7274 (2004).

[20] S. Baroni and R. Resta, Phys. Rev. B **33**, 7017 (1986).

[21] R. D. King-Smith and D. Vanderbilt, Phys. Rev. B **47**, 1651 (1993).

[22] A. Togo and I. Tanaka, Scr. Mater. **108**, 1 (2015).

[23] G. Yao, X. An, H. Lei, Y. Fu, and W. Wu, Model. Numer. Simul. Mater. Sci. **03**, 16 (2013).

[24] H. Liu, H.-k. Mao, M. Somayazulu, Y. Ding, Y. Meng, and D. Häusermann, Phys. Rev. B **70**, 094114 (2004).

[25] See Supplemental Material at http://link.aps.org/supplemental/10.1103/PhysRevB.106.064106 for details of (1) elastic stability criteria; (2) molecular dynamics simulations of ferroelectric AO; (3) superlattice of the rocksalt A_1O/A_2O.

[26] F. Mouhat and F.-X. Coudert, Phys. Rev. B **90**, 224104 (2014).

[27] H. Dixit, D. Lamoen, and B. Partoens, J. Phys.: Condens. Matter **25**, 035501 (2013).

[28] S. A. Khan, S. Azam, F. A. Shah, and B. Amin, Opt. Mater. **47**, 372 (2015).

[29] X. Yang, M. Hu, T. Su, X. Ma, Y. Chen, X. Kong, and W. Ren, J. Alloys Compd. **876**, 160167 (2021).

[30] S. Song, D. Kim, H. Jang, B. Yeo, S. S. Han, C. Kim, and J. Scott, Chem. Mater. **29**, 7596 (2017).

[31] F. A. Benko and F. P. Koffyberg, Solid State Commun. **57**, 901 (1986).

[32] P. D. C. King, T. D. Veal, A. Schleife, J. Zúñiga-Pérez, B. Martel, P. H. Jefferson, F. Fuchs, V. Muñoz-Sanjosé, F. Bechstedt, and C. F. McConville, Phys. Rev. B **79**, 205205 (2009).

[33] Z. R. Khan, M. Gandouzi, A. S. Alshammari, M. Bouzidi, M. Shkir, S. Alfaify, and M. Mohamed, J. Mater. Sci. Mater. Electron. **32**, 18304 (2021).

[34] Y. Yang, S. Jin, J. E. Medvedeva, J. R. Ireland, A. W. Metz, J. Ni, M. C. Hersam, A. J. Freeman, and T. J. Marks, J. Am. Chem. Soc. **127**, 8796 (2005).

[35] D. A. Cristaldi, S. Millesi, I. Crupi, G. Impellizzeri, F. Priolo, R. M. J. Jacobs, R. G. Egdell, and A. Gulino, J. Phys. Chem. C **118**, 15019 (2014).

[36] X. Li, T. A. Gessert, and T. Coutts, Appl. Surf. Sci. **223**, 138 (2004).

[37] K. J. Choi, M. Biegalski, Y. L. Li, A. Sharan, J. Schubert, R. Uecker, P. Reiche, Y. B. Chen, and X. Q. Pan, V. Gopalan *et al.*, Science **306**, 1005 (2004).

[38] S. Li and T. Birol, npj Comput. Mater. **6**, 168 (2020).

[39] H. Moriwake, R. Yokoi, A. Taguchi, T. Ogawa, C. A. J. Fisher, A. Kuwabara, Y. Sato, T. Shimizu, and Y. Hamasaki, H. Takashima *et al.*, APL Mater. **8**, 121102 (2020).

[40] O. G. Vendik and S. P. Zubko, J. Appl. Phys. **88**, 5343 (2000).

[41] K.-W. Lee and W. E. Pickett, Phys. Rev. B **68**, 085308 (2003).

[42] A. Kvasov, L. J. McGilly, J. Wang, Z. Shi, C. S. Sandu, T. Sluka, A. K. Tagantsev, and N. Setter, Nat. Commun. **7**, 12136 (2016).

[43] S. P. Beckman, X. Wang, K. M. Rabe, and D. Vanderbilt, Phys. Rev. B **79**, 144124 (2009).

[44] D. F. Crisler, J. J. Cupal, and A. R. Moore, Proc. IEEE **56**, 225 (1968).

[45] S. Liu and R. E. Cohen, Phys. Rev. Lett. **119**, 207601 (2017).

[46] F. Tasnadi, B. Alling, C. Hoglund, G. Wingqvist, J. Birch, L. Hultman, and I. A. Abrikosov, Phys. Rev. Lett. **104**, 137601 (2010).

[47] M. Akiyama, T. Kamohara, K. Kano, A. Teshigahara, Y. Takeuchi, and N. Kawahara, Adv. Mater. **21**, 593 (2009).

[48] P. S. Ghosh, S. Lisenkov, and I. Ponomareva, Phys. Rev. Lett. **125**, 207601 (2020).

[49] H. Wang, H. Liu, Z. Zhang, Z. Liu, Z. Lv, T. Li, W. Ju, H. Li, X. Cai, and H. Han, npj Comput. Mater. **5**, 17 (2019).

[50] D. G. Schlom, L.-Q. Chen, C. J. Fennie, V. Gopalan, D. A. Muller, X. Pan, R. Ramesh, and R. Uecker, MRS Bull. **39**, 118 (2014).

Correction: A grant number in the Acknowledgments contained an error and has been fixed.